talenta PUBLISHER

Journal of Technomaterial Physics
Journal homepage: https://talenta.usu.ac.id/JoTP

Tribological and Corrosion Performance of Reduced Graphene Oxide and Nanochitosan Reinforced Silicone Oil Coatings on Metal Surfaces

Ikhwanuddin[1]*, Yok Suprobo[1], Nurul Wahyuni[1], Markus Yando[1], Retno Sawitri Wulandari[1], and Zikri Noer[2,3,4]

[1]*Maritime Institute, Sekolah Tinggi Ilmu Pelayaran, North Jakarta, 14150, Indonesia*
[2]*Study Program of Instrumentation Engineering Technology, Faculty of Vocational, Universitas Sumatera Utara, Jl. Bioteknologi No. 2, Medan, 20155, North Sumatra, Indonesia*
[3]*Center of Excellence for Functional Materials and Instrumentation, Universitas Sumatera Utara, Medan, 20155, North Sumatra, Indonesia*
[4]*Department of Physics, Faculty of Mathematics and Natural Sciences, Universitas Sumatera Utara, Jl. Bioteknologi No. 1, Medan, 20155, North Sumatra, Indonesia*
*Corresponding Author: ikhwanudin@stipjakarta.ac.id

ARTICLE INFO

Article history:
Received 1 May 2026
Revised 13 August 2026
Accepted 15 August 2026
Available online 17 August 2026

E-ISSN: 2656-0755
P-ISSN: 2656-0747

How to cite:
Ikhwanuddin, Y. Suprobo, N. Wahyuni, M. Yando, R. S. Wulandari, and Z. Noer, "Tribological and Corrosion Performance of Reduced Graphene Oxide and Nanochitosan Reinforced Silicone Oil Coatings on Metal Surfaces," Journal of Technomaterial Physics, vol. 08, no. 02, pp. 131-146, Aug. 2026, doi: 10.32734/jotp.v8i2.25447.

ABSTRACT

Friction, wear, and corrosion critically affect the durability and reliability of metallic components in engineering and marine environments. Despite the established potential of reduced graphene oxide (rGO), nanochitosan, and silicone oil, their combined contribution within a multifunctional surface treatment remains insufficiently established. Here, an rGO/nanochitosan-reinforced silicone oil (PDMS) formulation was developed and assessed on aluminium and copper substrates through X-ray diffraction (XRD), surface roughness, coefficient of friction (CoF), wear rate, and corrosion rate measurements. XRD revealed rGO reflections at 2θ = 26.3° and 43.1° and nanochitosan reflections at 10.1° and 20.1°, with apparent crystallite sizes of 6.54–9.87 nm. The formulation containing 0.3 wt% rGO exhibited the most favorable response, lowering surface roughness, CoF, wear rate, and corrosion rate by approximately 40, 90, 86, and 90%, respectively, relative to uncoated surfaces. These findings establish a structure–performance relationship in the ternary rGO/nanochitosan/PDMS system, highlighting the role of optimized reinforcement content in achieving balanced tribological and corrosion resistance. The developed approach offers practical potential for metallic components operating under coupled mechanical and corrosive conditions.

Keywords: Corrosion, Nanochitosan, rGO, Tribofilm, Wear Resistance

ABSTRAK

Gesekan, keausan, dan korosi merupakan mekanisme degradasi utama yang memengaruhi ketahanan dan keandalan komponen logam pada lingkungan rekayasa dan maritim. Meskipun grafena oksida tereduksi (rGO), nanokitosan, dan minyak silikon (PDMS) telah menunjukkan potensi dalam perlindungan tribologi maupun korosi, kontribusi sinergis ketiganya dalam satu sistem pelapis multifungsi masih belum banyak dikaji. Penelitian ini mengembangkan formulasi minyak silikon yang diperkuat rGO/nanokitosan dan mengevaluasinya pada substrat aluminium dan tembaga melalui karakterisasi Difraksi Sinar-X (XRD), kekasaran permukaan, koefisien gesek (CoF), laju keausan, dan laju korosi. Hasil XRD menunjukkan refleksi rGO pada 2θ = 26,3° dan 43,1° serta refleksi nanokitosan pada 10,1° dan 20,1°, dengan ukuran kristalit semu 6,54–9,87 nm. Formulasi optimum dengan 0,3 wt% rGO menurunkan kekasaran permukaan, CoF, laju keausan, dan laju korosi masing-masing sekitar 40, 90, 86, dan 90% dibandingkan permukaan tanpa pelapisan. Temuan ini menunjukkan hubungan struktur–kinerja pada system terner rGO/nanokitosan/PDMS dan potensi penerapannya untuk perlindungan multifungsi komponen logam pada kondisi mekanis dan korosif secara simultan.

Kata kunci: Ketahanan Aus, Korosi, Nanokitosan, rGO, Tribofilm

1. Introduction

Friction, wear, and corrosion are the primary degradation mechanisms that reduce the durability, reliability, and efficiency of metallic components in mechanical and marine systems. Friction-related losses contribute approximately 20–23% of global energy dissipation in industrial machinery, while wear progressively damages surface integrity through material removal and increased surface roughness [1], [2]. In marine environments, seawater containing approximately 3.5 wt.% NaCl accelerates electrochemical reactions, causing corrosion rates of unprotected carbon steel to reach 0.1–0.3 mm $year^{-1}$ depending on exposure conditions [3]. The simultaneous interaction between mechanical deterioration and electrochemical attack, commonly referred to as tribocorrosion, intensifies surface degradation under sliding conditions. This issue is particularly critical in transportation and maritime industries because surface damage directly affects fuel efficiency, maintenance costs, and component lifetime. Consequently, the International Maritime Organization (IMO), through MARPOL Annex VI, promotes reducing energy consumption and greenhouse gas emissions in engineering systems. Therefore, multifunctional protective coatings capable of simultaneously reducing friction, suppressing wear, and improving corrosion resistance have become an important focus in advanced surface engineering.Silicone oil is widely utilized as a boundary lubricant because of its excellent thermal stability, chemical inertness, low surface tension, and flexible Si–O backbone structure [4]–[6]. Silicone oil possesses a density of approximately 965 kg m^{-3}, a viscosity ranging from 0.01 to 0.1 Pa.s, and a surface tension of approximately 20–21 mN m^{-1} [5]–[7]. These properties enable the formation of a stable lubricating film that minimizes asperity interactions and decreases the coefficient of friction to approximately 0.05–0.15 under boundary lubrication conditions [8], [9]. However, silicone oil exhibits limited load-bearing capability and insufficient anti-wear resistance under severe contact conditions.

To enhance protective performance, recent studies have incorporated nanostructured reinforcements into lubricant-based coatings. Among these materials, reduced graphene oxide (rGO) has attracted considerable attention because of its exceptional mechanical, thermal, and tribological properties. Reduced graphene oxide exhibits a specific surface area of approximately 2630 m^2 g^{-1}, a Young's modulus approaching 1.0–1.1 TPa, and thermal conductivity of up to 3000–5300 W m^{-1} K^{-1} [10], [11]. These characteristics enable rGO nanosheets to function as solid lubricants by reducing interfacial shear stress and promoting the formation of low-shear tribofilms during sliding [12]–[18]. Moreover, the compact layered structure of rGO effectively inhibits the penetration of oxygen, moisture, and chloride ions, thereby improving corrosion resistance in aggressive environments [19]–[23]. Nevertheless, excessive rGO incorporation frequently causes nanosheet agglomeration because of strong van der Waals interactions, resulting in poor dispersion stability and reduced coating uniformity [24]. Besides graphene-based nanomaterials, nanochitosan has emerged as a promising environmentally friendly reinforcing material because of its excellent film-forming capability and strong affinity toward metallic substrates [25], [26]. Nanochitosan generally exhibits particle sizes ranging from 50 to 100 nm with specific surface areas of approximately 80–150 m^2 g^{-1} depending on the synthesis route [27]–[29]. The abundant amine ($–NH_2$) and hydroxyl (–OH) functional groups facilitate adsorption, chelation, and hydrogen-bonding interactions at the coating–metal interface [30]–[36]. Previous investigations reported that nanochitosan coatings improved corrosion inhibition efficiency by approximately 40–65% through compact protective layer formation and enhanced coating adhesion [31]–[33]. However, despite these advantages, nanochitosan-based systems generally exhibit limited mechanical strength and insufficient resistance under severe tribological loading [30]. Recent studies have demonstrated the potential of rGO-based coatings, silicone oil lubricants, and nanochitosan-derived protective systems for tribological and corrosion protection. Ye et al. [15] reported that rGO-reinforced coatings reduced wear rates by approximately 72% because of stable tribofilm formation and improved load-bearing capability. Sharma et al. [19] showed that rGO-filled polymer coatings enhanced corrosion resistance by more than 55% through the barrier effect of graphitic layers against oxygen and chloride ion diffusion. Mishra et al. [37] demonstrated that nanochitosan-based coatings significantly improved corrosion inhibition through adsorption and chelation mechanisms involving amine and hydroxyl functional groups. Wang et al. [8] further reported that silicone oil lubricants reduced friction coefficients to approximately 0.06–0.12 under boundary lubrication conditions owing to stable lubricating film formation.

Although these studies demonstrated promising tribological and corrosion performance, they primarily focused on individual materials or binary composite systems. Most investigations involving rGO emphasized tribofilm formation and wear reduction, whereas nanochitosan studies mainly focused on corrosion inhibition and interfacial adhesion. Similarly, silicone oil studies primarily investigated lubrication performance without incorporating multifunctional nanoscale reinforcements. Consequently, the synergistic effects of combining rGO, nanochitosan, and silicone oil within a single multifunctional coating architecture remain insufficiently understood. Furthermore, the relationship between crystallographic characteristics, interfacial interactions,

tribofilm formation, and the resulting tribological and corrosion performance has not been comprehensively investigated.

Therefore, this study addresses these knowledge gaps by developing a multifunctional silicone oil coating reinforced with reduced graphene oxide (rGO) and nanochitosan for metallic surface protection. Unlike previous studies that evaluated these materials individually or in binary combinations, the present work systematically integrates rGO, nanochitosan, and silicone oil into a unified coating system and correlates its crystallographic characteristics with surface roughness, coefficient of friction, wear resistance, and corrosion performance under identical experimental conditions. This integrated approach provides new insight into the synergistic reinforcement mechanism governing multifunctional surface protection and contributes to the development of environmentally friendly protective coatings for engineering and marine applications requiring simultaneous lubrication, wear resistance, and corrosion protection. Accordingly, the developed coating was deposited on aluminium and copper substrates, and its crystallographic characteristics, tribological behaviour, and corrosion resistance were systematically evaluated under identical experimental conditions.

2. Method

2.1. Materials

The materials used in this study included silicone oil (1000 cP, Inosol), graphite powder as the precursor for reduced graphene oxide (rGO), nanochitosan, and aluminium (Al) and copper (Cu) substrates. The chemical reagents consisted of sulfuric acid (H_2SO_4, 98%), sodium nitrate ($NaNO_3$), potassium permanganate ($KmnO_4$), hydrogen peroxide (H_2O_2, 30%), cetyltrimethylammonium bromide (CTAB), sodium borohydride ($NaBH_4$), sodium hydroxide (NaOH), sodium tripolyphosphate (NaTPP), Tween 80, hydrochloric acid (HCl), ethanol, and acetic acid.

2.2. Synthesis of rGO

Reduced graphene oxide (rGO) was synthesized via a modified Hummers method followed by surfactant-assisted exfoliation and chemical reduction, adapted from previous graphene exfoliation and graphene-processing studies [10], [11], [38]. Initially, 1 g of graphite powder and 50 mg of $NaNO_3$ were added to 70 mL of concentrated H_2SO_4 (98%) under ice-bath conditions to maintain the reaction temperature below 20 °C. Subsequently, 3 g of $KMnO_4$ was gradually introduced under continuous stirring for 2 h at approximately 20 °C to initiate the oxidation process. After removing the ice bath, the mixture was stirred for 24 h at room temperature to ensure complete oxidation. The suspension was then diluted with deionized (DI) water under stirring for 1 h, followed by the addition of 30% H_2O_2 to terminate the oxidation reaction. The resulting graphite oxide was filtered and washed sequentially with dilute HCl and DI water until a neutral pH was achieved. The obtained graphite oxide was dispersed in deionized water and exfoliated into graphene oxide (GO) through ultrasonication (50/60 Hz) for 90 min, producing GO nanosheets. Subsequently, 100 mg of GO dispersion was re-dispersed in 100 mL DI water and sonicated to ensure homogeneity. For surfactant modification, 2 g of cetyltrimethylammonium bromide (CTAB), previously dissolved in 100 mL ethanol, was added to the GO dispersion and stirred for 24 h at room temperature. Chemical reduction was then carried out by adding $NaBH_4$ solution (1% in 0.2% NaOH) under continuous stirring in a water bath for 24 h. The formation of a black precipitate indicated the successful reduction of graphene oxide into reduced graphene oxide (rGO). The product was filtered, washed repeatedly with a water–ethanol (1:1) mixture, and dried at 60 °C for 72 h.

2.3. Synthesis of Nanochitosan

Nanochitosan was synthesized using the ionic gelation method adapted from previous studies [27], [28]. Chitosan powder (0.05% w/v) was dissolved in 100 mL of 1% (w/v) acetic acid and stirred using a magnetic stirrer for 1 h until completely dissolved. Subsequently, NaTPP (0.1% w/v) and Tween 80 (0.1% v/v) were added to the chitosan solution at a ratio of 5:1:0.05 under continuous stirring. The mixture was stirred at room temperature for 2 h and then subjected to ultrasonication for 30 min [19]. The resulting suspension was dried using a spray dryer to obtain nanochitosan particles in powder form.

2.4. Preparation of rGO and Nanochitosan Reinforced Silicone Oil Coatings

The coating formulation was prepared by dispersing reduced graphene oxide (rGO) and nanochitosan into silicone oil as the coating matrix. The composition variations were arranged using a completely randomized non-factorial design, as presented in Table 1. A predetermined amount of rGO and nanochitosan was gradually added into 100 mL of silicone oil under magnetic stirring at 25 °C with a stirring speed of 600 rpm for 24 h to ensure homogeneous dispersion. The suspension was subsequently stirred for an additional 2 h and

ultrasonicated for 30 min to minimize rGO agglomeration and obtain a homogeneous coating suspension prior to deposition. Stable rGO dispersion is essential for maintaining rheological stability and preventing nanosheet agglomeration within lubricant systems [39]. The prepared suspension was then deposited onto cleaned metal substrates using a spray-coating technique and allowed to dry at room temperature for 24 h before characterization and performance evaluation.

Table 1. Composition of silicone oil–rGO–nanochitosan coatings.

No	Sample Code	Silicone Oil (mL)	rGO (wt%)	Nanochitosan (wt%)
1	S0	100	0.0	0.0
2	S1	100	0.1	0.1
3	S2	100	0.3	0.1
4	S3	100	0.5	0.3
5	S4	100	0.7	0.5

2.5. Characterization, Tribological, and Corrosion Testing

Aluminium (Al) and copper (Cu) plates (5 cm × 5 cm) were used as substrates. Before coating, the metal surfaces were cleaned, degreased, and dried. The prepared silicone oil–rGO–nanochitosan suspension was uniformly applied onto the substrate surfaces using a spray-coating method to form a protective coating layer. The crystallographic structure and phase composition were characterized using X-ray diffraction (XRD) with Cu-Kα radiation (λ = 0.15406 nm) over a scanning range of 2θ = 5°–80°. The apparent crystallite size associated with the individual diffraction peaks was estimated using the Debye–Scherrer equation based on the full width at half maximum (FWHM), representing the coherent diffraction domain size rather than the actual particle size. The coated specimens were further evaluated for surface roughness, coefficient of friction (CoF), wear rate, corrosion rate, and qualitative corrosion behaviour using a stylus profilometer, reciprocating tribometer, and potentiostat in accordance with the relevant ASTM standards. Each experimental measurement was performed in triplicate (n = 3). The experimental data were analysed using descriptive statistics and are reported as the mean ± standard deviation (SD) of three independent measurements. The error bars shown in all graphical results represent one standard deviation calculated from these independent measurements.

The overall experimental procedure employed in this study is summarized in Figure 1. The workflow consists of the synthesis of reduced graphene oxide (rGO) and nanochitosan, preparation of the silicone oil–rGO–nanochitosan coating, deposition onto metallic substrates, followed by crystallographic, tribological, and corrosion characterization.

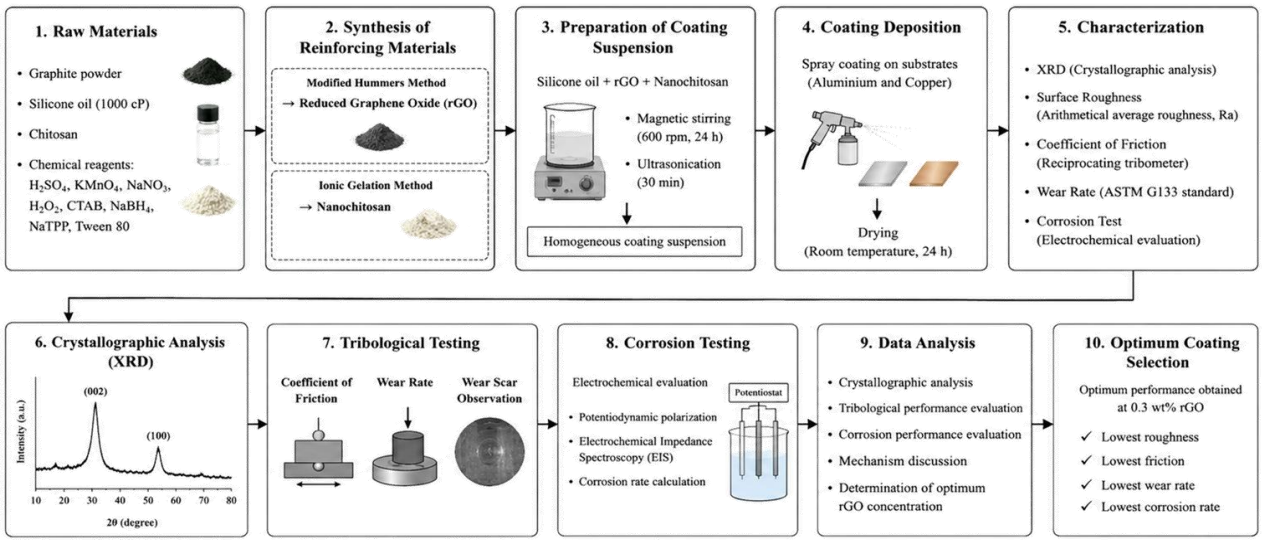

Figure 1. Experimental workflow for the synthesis, preparation, deposition, characterization, and performance evaluation of the rGO/nanochitosan reinforced silicone oil coating.

3. Results and Discussion

3.1. X-ray Diffraction (XRD) Analysis

The phase structure, crystallinity behavior, and nanocrystalline characteristics of the reduced graphene oxide (rGO)/nanochitosan reinforced silicone oil coating were investigated using X-ray diffraction (XRD) analysis. The XRD characterization was performed to verify the successful incorporation of reduced graphene oxide (rGO), nanochitosan, and silicone oil (PDMS) into the multifunctional tribological and corrosion-resistant coating system developed for metallic surface protection.

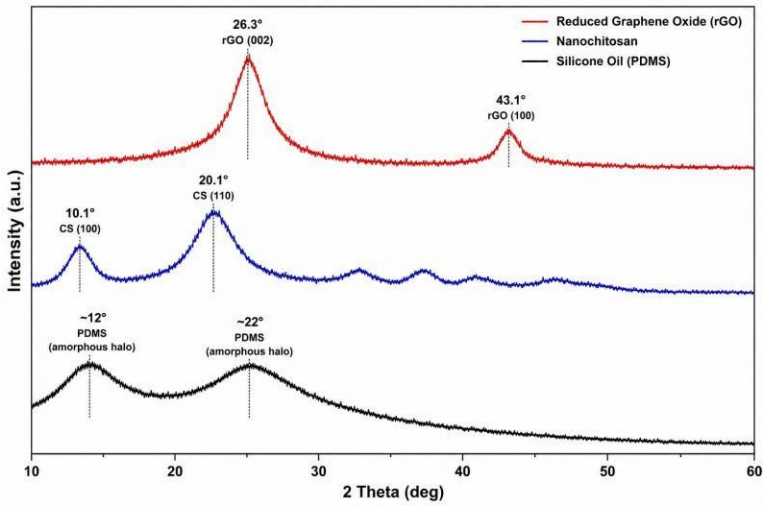

Figure 2. XRD patterns of reduced graphene oxide (rGO), nanochitosan, and silicone oil (PDMS).

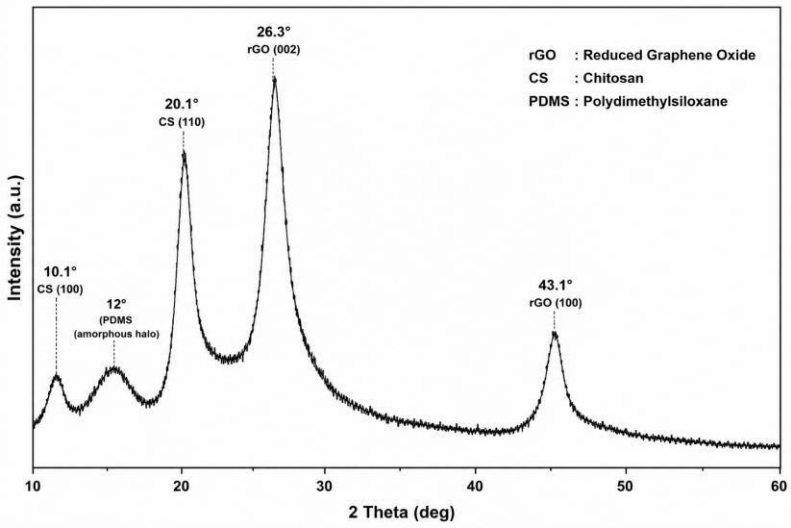

Figure 3. XRD pattern of the optimum rGO/nanochitosan-reinforced silicone oil coating containing 0.3 wt% rGO deposited on the metallic substrate.

The diffraction pattern of rGO exhibited a dominant diffraction peak at $2\theta = 26.3°$, corresponding to the (002) crystallographic plane of graphitic carbon. This peak is characteristic of graphitic layered structures and indicates the partial restoration of ordered graphitic domains following the reduction of graphene oxide. A secondary diffraction peak observed at $2\theta = 43.1°$ was indexed to the (100) crystallographic plane, representing the in-plane ordering of sp^2-hybridized carbon networks. Similar diffraction features have been widely reported for reduced graphene oxide and graphene-derived nanostructures [10], [11], [18]. The relatively broad diffraction profile of the rGO phase indicates reduced coherent diffraction domains and increased structural disorder, which are characteristic of nanocrystalline graphitic materials. The peak broadening also suggests the formation of few-layer rGO nanosheets with high surface activity and improved interfacial interaction capability within the polymeric coating matrix. Furthermore, the shift and broadening of the graphitic peak relative to pristine graphite indicate partial exfoliation and defect generation during the oxidation–reduction

process. Nanochitosan exhibited two characteristic diffraction peaks centered at 2θ = 10.1° and 20.1°, corresponding to the semi-crystalline (100) and (110) planes of chitosan, respectively. The diffraction peak near 10° is generally associated with hydrated crystalline domains, whereas the stronger peak around 20° originates from intermolecular hydrogen-bonding interactions among chitosan molecular chains [27], [35], [36]. The broadening of these diffraction peaks indicates reduced crystallinity and the formation of nanocrystalline domains after ionic gelation. Compared with commercial chitosan, the decrease in diffraction intensity and peak broadening suggest disruption of the ordered molecular arrangement following nanoscale modification. Such structural changes improve polymer flexibility, dispersion stability, and interfacial compatibility within multifunctional coating systems [28], [35], [36]. The silicone oil (PDMS) phase exhibited a broad amorphous halo within the 2θ range of approximately 12–22°, confirming the predominantly amorphous nature of the polymer matrix. Silicone-based polymers generally possess low crystallinity because of the flexible siloxane backbone and random molecular orientation of polydimethylsiloxane chains [9], [40], [41]. The absence of distinct crystalline peaks indicates that PDMS primarily functions as an amorphous lubricating matrix within the developed coating system.

Following the incorporation of rGO and nanochitosan into the silicone oil matrix, the optimum composite coating containing 0.3 wt% rGO exhibited diffraction features corresponding to graphitic carbon, semi-crystalline chitosan, and amorphous PDMS, as presented in Figure 2. The persistence of the rGO (002) diffraction peak at 26.3° demonstrates that the graphitic structure remained stable after composite formation. Nevertheless, the diffraction peaks became broader and partially overlapped, indicating enhanced interfacial interactions and improved dispersion between rGO nanosheets, nanochitosan particles, and PDMS chains. These observations suggest that the composite structure is primarily governed by physical interactions, including hydrogen bonding, van der Waals attraction, and π–π stacking interactions between rGO sheets and chitosan polymer chains [24][36]. Such interfacial interactions are expected to improve coating compactness, mechanical integrity, and protective performance under tribological and corrosive environments [42].

To further evaluate the crystallographic characteristics of the synthesized materials, the apparent crystallite size was estimated using the Debye–Scherrer equation [43]:

$$D = \frac{K\lambda}{\beta \cos\theta} \tag{1}$$

where D is the apparent crystallite size (nm), K is the Scherrer constant (0.94), λ is the wavelength of Cu-Kα radiation (0.15406 nm), β is the full width at half maximum (FWHM), and θ is the Bragg diffraction angle. The lattice microstrain was calculated using:

$$\varepsilon = \frac{\beta}{4\tan\theta} \tag{2}$$

where ε is the microstrain, β is the diffraction peak broadening, and θ is the Bragg angle.

Table 2. Crystallographic parameters of the rGO/nanochitosan reinforced silicone oil coating.

Material	Peak Position (2θ)	Plane/Phase	FWHM (β)	Crystallite Size (nm)	Microstrain (×10^{-3})
Reduced Graphene Oxide	26.3°	G (002)	1.233°	6.91	23.03
	43.1°	G (100)	1.083°	8.24	11.96
Nanochitosan	10.1°	CS (100)	0.844°	9.87	41.67
	20.1°	CS (110)	1.134°	7.43	27.92
Silicone Oil (PDMS)	12–22°	Amorphous halo	-	-	-
rGO/Nanochitosan/PDMS Composite Coating	26.3°	rGO (002)	1.287°	6.54	24.81

The calculated apparent crystallite sizes of rGO and nanochitosan ranged from 6.91 to 9.87 nm, indicating the presence of nanocrystalline domains within the synthesized reinforcing materials. After incorporation into the silicone oil matrix, the apparent crystallite size calculated from the rGO (002) diffraction peak decreased to approximately 6.54 nm, suggesting stronger structural confinement and enhanced interfacial interactions

between the dispersed rGO nanosheets, nanochitosan particles, and the PDMS matrix. The corresponding increase in lattice microstrain indicates the development of structural distortion associated with improved interfacial bonding within the hybrid coating. The observed structural refinement is expected to improve coating compactness, reduce structural defects, strengthen interfacial adhesion, and enhance barrier resistance against corrosive species, thereby contributing to the improved tribological and corrosion performance of the developed coating system [13], [19], [20], [21], [22], [23]. It should be noted that the Debye–Scherrer equation estimates the coherent diffraction domain size rather than the actual particle size. Therefore, complementary characterization techniques such as transmission electron microscopy (TEM), dynamic light scattering (DLS) or particle size analysis (PSA), and Raman spectroscopy are recommended in future studies to further verify particle morphology, size distribution, and the structural characteristics of the synthesized rGO.

3.2. Surface Roughness

Surface roughness was quantitatively evaluated using a stylus profilometer on aluminium (Al) and copper (Cu) substrates in accordance with ISO 4287/4288 standards to characterize the surface topography after coating deposition. The roughness parameters Ra, Rq, and Rz were selected because they represent complementary aspects of surface morphology. Specifically, Ra represents the arithmetic mean deviation of the surface profile, Rq (root mean square roughness) is more sensitive to peak–valley fluctuations, whereas Rz represents the maximum peak-to-valley height and is particularly useful for assessing severe asperities that influence tribological contact behavior [44], [45]. The reported values represent the average roughness obtained from repeated measurements on each coated specimen. The uncoated substrates exhibited Ra values of 0.235 µm (Cu) and 0.268 µm (Al), which decreased to 0.198 µm (Cu) and 0.226 µm (Al) after the application of the silicone oil coating, corresponding to reductions of approximately 15.7% for both substrates. This improvement demonstrates that the silicone oil layer effectively modified the initial surface profile. The reduction in roughness is associated with the relatively low surface tension of silicone oil (20–21 mN m^{-1}), which promotes uniform spreading over metallic surfaces, fills microscale surface valleys, and redistributes local contact stresses under boundary lubrication conditions [5]–[7], [31]. The variation of surface roughness parameters as a function of reduced graphene oxide (rGO) concentration is presented in Figure 4.

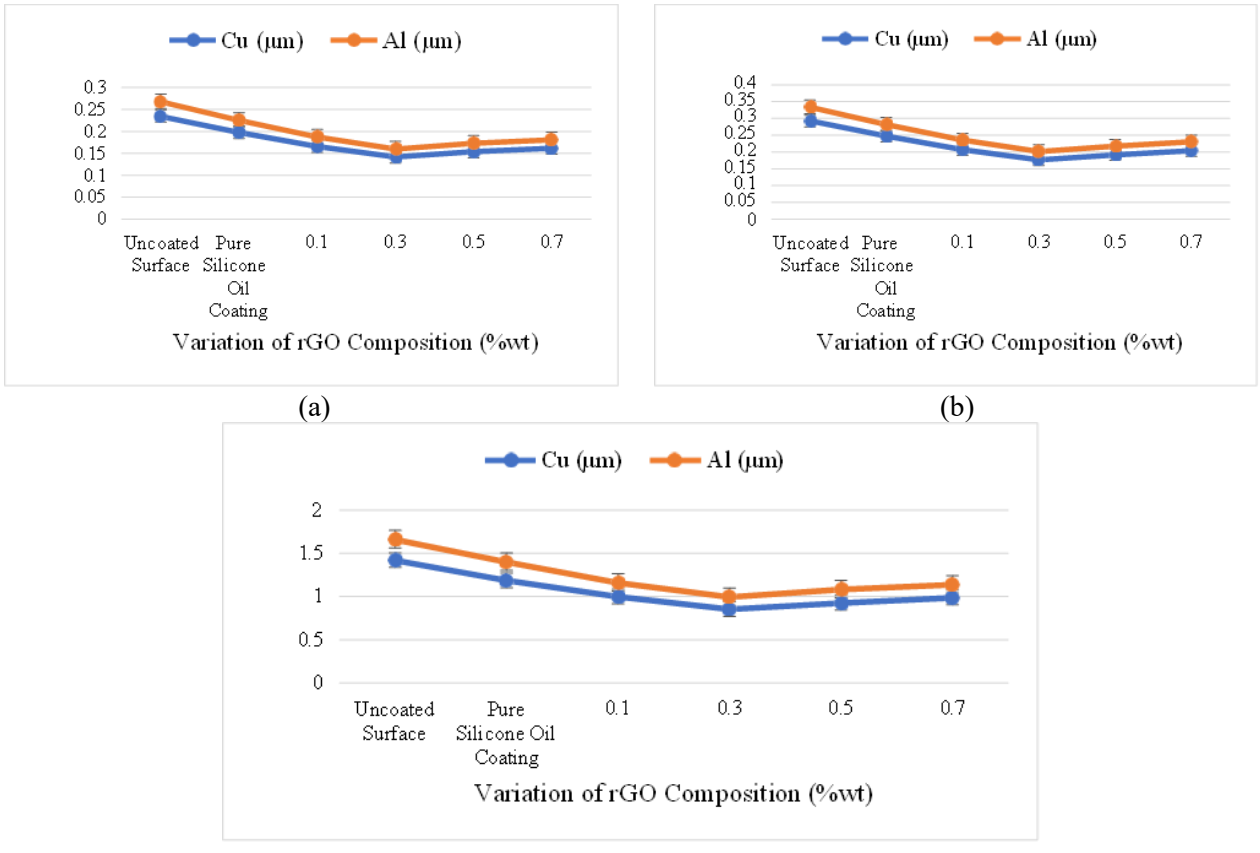

Figure 4. Effect of rGO concentration on surface roughness parameters (a) Ra, (b) Rq, and (c) Rz for Cu and Al substrates.

As shown in Figure 4, all surface roughness parameters (Ra, Rq, and Rz) decreased progressively with increasing rGO concentration up to 0.3 wt%, followed by a slight increase at higher concentrations. The optimum performance was obtained at 0.3 wt% rGO, where Ra decreased to 0.142 µm (Cu) and 0.161 µm (Al), corresponding to reductions of 39.6% and 39.9%, respectively, compared with the uncoated substrates. Similar trends were observed for Rq and Rz, indicating not only a reduction in the average surface roughness but also suppression of pronounced surface asperities. The improvement in surface smoothness is attributed to the uniform dispersion of rGO nanosheets within the silicone oil matrix, which effectively fills microscale surface valleys and promotes the formation of a continuous protective tribofilm during coating deposition. In addition, the layered structure of rGO facilitates stress redistribution over the contact surface, thereby producing a more homogeneous coating with reduced surface irregularities. These observations are consistent with previous reports describing the ability of rGO to improve coating compactness and surface uniformity through nanoscale reinforcement [13]-[15], [17], [18]. However, when the rGO concentration exceeded the optimum level (0.5–0.7 wt%), the roughness parameters increased slightly. The Ra values increased to 0.154–0.162 µm (Cu) and 0.174–0.182 µm (Al), representing an increase of approximately 8–14% relative to the optimum condition. This behavior is attributed to the agglomeration of rGO nanosheets caused by strong van der Waals interactions, resulting in non-uniform dispersion and localized surface irregularities. Similar behavior has been reported for rGO/polymer nanocomposite coatings, in which excessive rGO loading reduces coating homogeneity because of nanosheet agglomeration [24], [36].

Nanochitosan also contributed to the improved coating performance by enhancing film compactness and interfacial adhesion. The abundant hydroxyl (–OH) and amine ($–NH_2$) functional groups facilitate adsorption onto metallic substrates and strengthen the interaction between the reinforcing phases and the PDMS matrix through hydrogen bonding. Consequently, nanochitosan assists in reducing coating defects and improving coating integrity, consistent with previous studies on chitosan-based protective coatings [31]–[33]. Furthermore, aluminium consistently exhibited higher roughness values than copper under all coating conditions. This difference is attributed to the higher chemical reactivity and stronger tendency of aluminium to form oxide layers, which may influence coating spreading behavior and surface uniformity. Overall, the simultaneous reduction of Ra, Rq, and Rz demonstrates that the rGO/nanochitosan reinforced silicone oil coating effectively modified the substrate surface by reducing asperity height and minimizing severe surface irregularities. The optimum performance observed at 0.3 wt% rGO indicates an appropriate balance between efficient nanosheet dispersion, effective asperity filling, and coating compactness. These characteristics provide a smoother contact interface that is expected to contribute to lower friction, reduced wear, and improved corrosion resistance, as discussed in the subsequent sections.

3.3. Coefficient of Friction

The coefficient of friction (CoF, μ) represents the cumulative response of microscale interactions occurring at the sliding interface between two contacting surfaces. The tribological performance of the developed coating was evaluated using a reciprocating tribometer under a normal load of 12.72 kg, a test duration of 60 s, and a sliding distance of 30 cm. The reported CoF values are presented as mean ± standard deviation (SD). The uncoated substrate exhibited a CoF of 0.249 ± 0.008, which decreased markedly to 0.051 ± 0.004 after the application of the silicone oil coating, corresponding to a reduction of approximately 79.5%. This substantial decrease demonstrates the ability of the silicone oil layer to minimize direct asperity-to-asperity contact by forming a lubricating boundary film that separates the contacting surfaces during sliding [6]–[9]. The variation in the coefficient of friction as a function of reduced graphene oxide (rGO) concentration is presented in Figure 5.

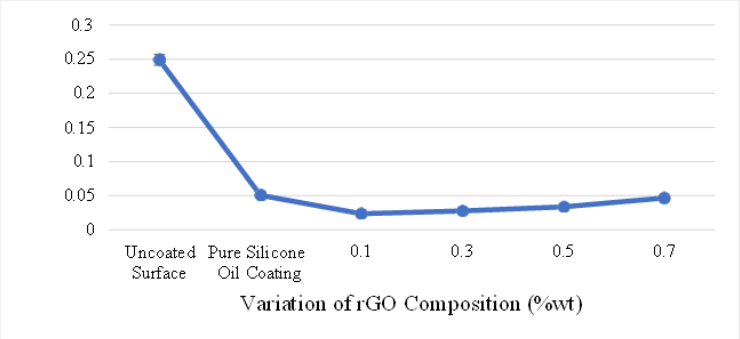

Figure 5. Effect of rGO concentration on the coefficient of friction of silicone oil–rGO–nanochitosan coatings. Error bars represent the standard deviation (n = 3).

As shown in Figure 5, the incorporation of rGO further reduced the coefficient of friction, with the optimum performance obtained at 0.3 wt% rGO, where the CoF reached 0.024 ± 0.002. This value corresponds to reductions of approximately 90.4% relative to the uncoated substrate and 52.9% compared with the silicone oil coating without rGO. The optimum friction reduction agrees well with the surface roughness results, where 0.3 wt% rGO also produced the lowest Ra, Rq, and Rz values. This correlation indicates that the reduction in friction is governed not only by improved surface smoothness but also by the formation of a stable low-shear tribofilm. The enhanced tribological performance can be attributed to the unique layered structure of rGO nanosheets, which function as solid lubricants during sliding. Under repeated contact, the nanosheets tend to align parallel to the sliding direction, facilitating interlayer sliding and reducing interfacial shear stress. Simultaneously, dispersed rGO fills microscale surface valleys, producing a more uniform contact interface and reducing localized stress concentrations. Previous studies have similarly reported that rGO reduces friction through tribofilm formation, interlayer sliding, and boundary lubrication mechanisms [13]–[18]. In addition, friction-reducing nanofillers have been reported to improve tribological performance through synergistic interactions within lubricating boundary films [46].

At a lower concentration (0.1 wt% rGO), the coefficient of friction decreased to 0.032 ± 0.003, indicating that although rGO contributed to lubrication, the nanosheet concentration was insufficient to establish a continuous and stable tribofilm over the entire contact interface. Conversely, increasing the rGO concentration beyond the optimum level (0.5 wt% and 0.7 wt%) resulted in the CoF increasing to 0.031 ± 0.003 and 0.045 ± 0.005, respectively. This deterioration is consistent with the surface roughness results and is attributed to the agglomeration of rGO nanosheets caused by strong van der Waals interactions. Agglomeration reduces dispersion uniformity, creates localized contact asperities, and disrupts the continuity of the lubricating tribofilm, thereby increasing friction. Similar observations have been reported for rGO/polymer nanocomposite lubricants, in which excessive rGO loading adversely affects tribological performance because of unstable nanosheet dispersion. Nanochitosan also contributes to the tribological performance by improving coating cohesion and interfacial adhesion. The abundant hydroxyl (–OH) and amine ($–NH_2$) functional groups promote strong adsorption onto metallic substrates and facilitate hydrogen-bonding interactions within the hybrid coating structure. These interactions enhance coating compactness and improve tribofilm stability during repeated sliding, thereby supporting the friction-reducing effect of rGO [31]–[33]. Overall, the lowest coefficient of friction obtained at 0.3 wt% rGO (0.024 ± 0.002) is attributed to the synergistic effects of reduced surface roughness, homogeneous rGO dispersion, efficient interlayer sliding of rGO nanosheets, and enhanced coating cohesion provided by nanochitosan. These results demonstrate that 0.3 wt% rGO provides the optimum balance between surface smoothing, tribofilm stability, and dispersion homogeneity, thereby producing the most effective tribological performance among the investigated coating formulations.

3.4. Wear Rate

The wear rate was evaluated to assess the wear resistance of the developed coating under repeated sliding conditions. The measurements were performed using a reciprocating tribometer in accordance with ASTM G133 (linearly reciprocating ball-on-flat sliding wear test). The wear rate was determined from the material loss during sliding and represents the resistance of the coated surface to mechanical degradation under boundary lubrication conditions.

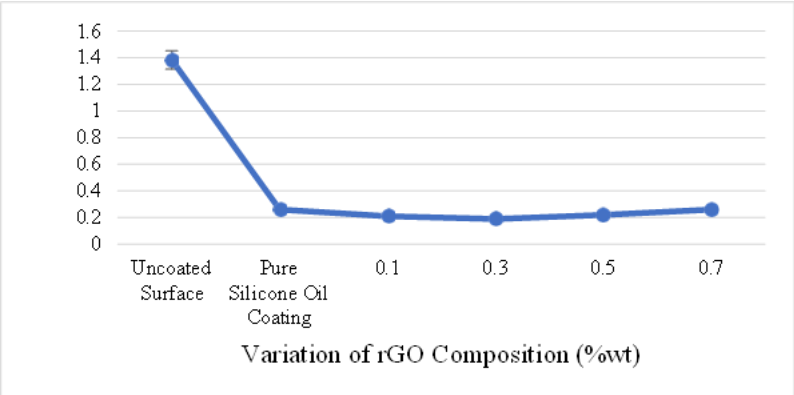

Figure 6. Effect of rGO concentration on the wear rate of the silicone oil–rGO–nanochitosan coatings.

The wear rate decreased significantly from 1.382 for the uncoated substrate to 0.260 after the application of the silicone oil coating, corresponding to an 81.2% reduction. This improvement indicates that the silicone

oil layer effectively reduced direct metal-to-metal contact by forming a lubricating boundary film, thereby suppressing severe adhesive and abrasive wear. The incorporation of reduced graphene oxide (rGO) further enhanced the wear resistance of the coating. The lowest wear rate (0.190) was obtained at 0.3 wt% rGO, corresponding to an 86.3% reduction compared with the uncoated substrate. The variation in wear rate as a function of rGO concentration is presented in Figure 6. The wear-rate trend closely follows the variations observed in surface roughness and coefficient of friction. The optimum composition (0.3 wt% rGO) simultaneously produced the lowest roughness, the minimum coefficient of friction, and the highest wear resistance. These observations indicate that wear reduction results from the combined effects of surface smoothing, reduced interfacial shear stress, and improved load distribution during sliding. The enhanced wear resistance can be explained by the synergistic interaction between the silicone oil matrix, uniformly dispersed rGO nanosheets, and nanochitosan. Under boundary lubrication conditions, silicone oil forms a lubricating film that minimizes direct metal-to-metal contact, whereas the layered structure of rGO promotes the formation of a protective tribofilm with low shear resistance [47], [48]. The graphitic layers facilitate interlayer sliding and simultaneously act as a load-bearing barrier, thereby reducing plastic deformation and material removal during repeated sliding. Previous studies have similarly reported that rGO-based tribofilms improve wear resistance through low-shear sliding, enhanced load-carrying capability, and effective surface protection mechanisms [13]–[18]. Nanochitosan further contributes by improving coating compactness and interfacial adhesion. The abundant hydroxyl (–OH) and amine ($–NH_2$) functional groups strengthen the interaction between the reinforcing phases and the metallic substrate, thereby enhancing coating integrity and reducing tribofilm delamination during repeated sliding [31]–[33]. The proposed tribological mechanism responsible for the enhanced wear resistance is illustrated schematically in Figure 7.

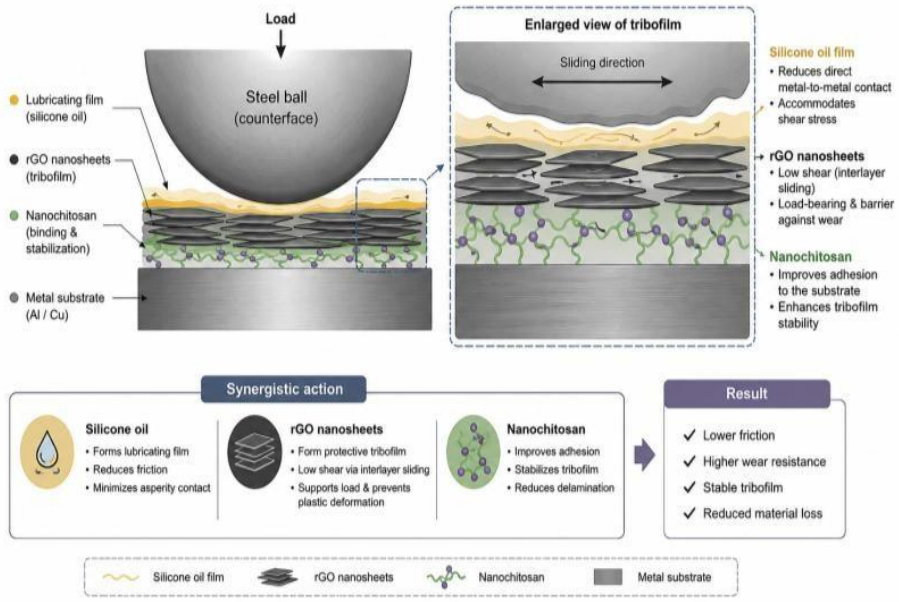

Figure 7. Schematic illustration of the proposed tribological mechanism of the silicone oil–rGO–nanochitosan coating under boundary lubrication conditions.

As illustrated in Figure 7, silicone oil initially forms a lubricating boundary film that reduces direct asperity contact. Meanwhile, uniformly dispersed rGO nanosheets gradually develop a continuous tribofilm capable of reducing interfacial shear stress while redistributing the applied load across the contact surface. Nanochitosan enhances coating compactness and interfacial adhesion, thereby improving tribofilm stability and minimizing material removal during repeated sliding. However, increasing the rGO concentration beyond the optimum level (0.5–0.7 wt%) resulted in a gradual increase in wear rate to 0.220–0.260. This deterioration is attributed to the agglomeration of rGO nanosheets caused by strong van der Waals interactions, leading to non-uniform dispersion within the coating. Agglomerated particles interrupt the continuity of the protective tribofilm and may act as third-body abrasive particles during sliding, thereby accelerating material removal. Similar behavior has been reported for rGO/polymer nanocomposite coatings, where excessive rGO loading promotes nanosheet agglomeration and unstable tribofilm formation [24]. The influence of rGO dispersion on tribofilm formation at different reinforcement concentrations is illustrated schematically in Figure 8.

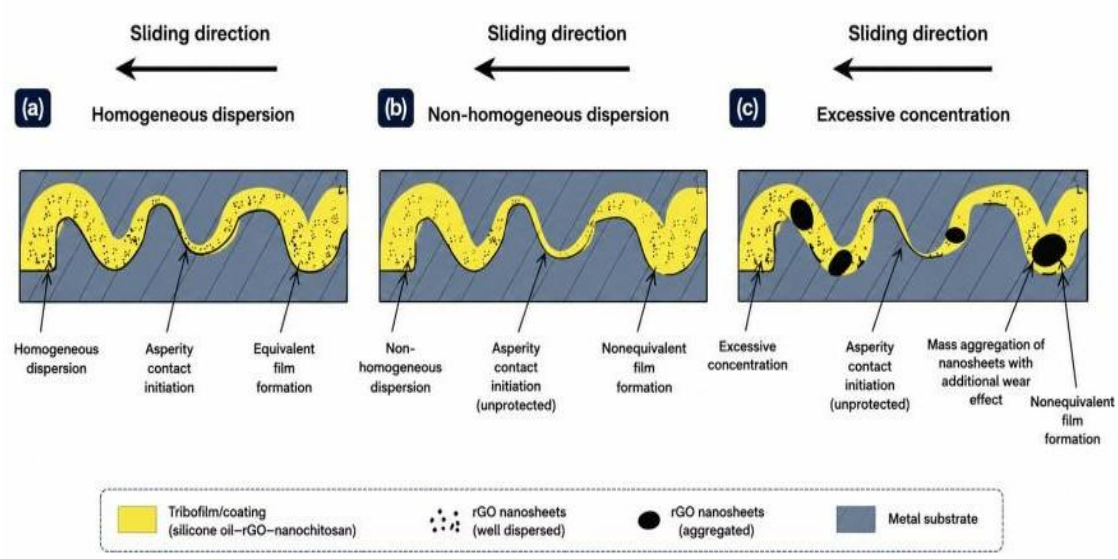

Figure 8. Schematic illustration of tribofilm formation and dispersion behavior of rGO–nanochitosan in the silicone oil matrix under sliding conditions [18].

Figure 8 demonstrates that homogeneous rGO dispersion promotes the formation of a continuous tribofilm capable of uniformly distributing the applied load and protecting the substrate surface. In contrast, excessive rGO loading leads to nanosheet agglomeration, discontinuous tribofilm formation, localized stress concentrations, and consequently higher wear rates. These observations are in good agreement with the experimental wear-rate results and further explain why the optimum tribological performance was achieved at 0.3 wt% rGO.

3.5. Corrosion Type Analysis

The corrosion type analysis was conducted to evaluate the corrosivity of the developed coating formulations toward metallic materials using the Copper Strip Corrosion Test in accordance with ASTM D130. This method assesses the degree of discoloration and tarnishing on polished copper strips after exposure to the test solution under controlled conditions, providing a qualitative evaluation of the corrosive characteristics of lubricating fluids.

Table 3. Corrosion type classification of the silicone oil–rGO–nanochitosan coating formulations according to ASTM D130.

Coating Solution Type	Corrosion Rating
Silicone Oil	1a (Slight Tarnish)
0.1 wt%	1a (Slight Tarnish)
0.3 wt%	1a (Slight Tarnish)
0.5 wt%	1a (Slight Tarnish)
0.7 wt%	1a (Slight Tarnish)

The results demonstrate that all coating formulations exhibited a 1a (slight tarnish) classification, indicating only minimal surface discoloration without visible corrosion products or severe surface deterioration. According to ASTM D130, this rating represents excellent chemical compatibility between the lubricant formulation and copper surfaces, confirming that the developed coating system is essentially non-corrosive under the applied test conditions. The consistently low corrosivity is attributed primarily to the barrier properties of the silicone oil–rGO–nanochitosan coating system. Silicone oil provides a hydrophobic lubricating film that limits the contact between the metallic surface and the surrounding environment, thereby reducing the accessibility of corrosive species. In addition, the layered structure of reduced graphene oxide (rGO) increases the diffusion path of oxygen, moisture, and chloride ions, enhancing the barrier performance of the coating. Similar barrier effects have been widely reported for graphene-based protective coatings used in tribological and anti-corrosion applications [19]–[23], [49].

Nanochitosan further contributes to coating performance by improving coating compactness and interfacial

adhesion through its abundant hydroxyl (–OH) and amine ($–NH_2$) functional groups. The improved coating integrity reduces coating defects that may otherwise facilitate the penetration of corrosive species. Previous studies have similarly reported that chitosan-based protective coatings improve corrosion resistance by forming compact surface films and enhancing coating stability [30]–[33]. The identical 1a classification obtained for all formulations indicates that the incorporation of rGO and nanochitosan does not introduce additional corrosive characteristics into the silicone oil matrix. Instead, the hybrid coating maintains excellent chemical stability while simultaneously providing tribological benefits, making it a promising multifunctional coating for engineering and marine applications where both wear resistance and corrosion protection are required.

3.6. Corrosion Rate Analysis

The corrosion rate was evaluated using a potentiostat in accordance with ASTM G59 under three corrosive environments, namely 3.5 wt.% NaCl solution, natural seawater, and 3 wt.% H_2SO_4, to assess the corrosion resistance of the developed coatings. The corrosion rate was used to quantify the degradation behaviour of the coated metallic substrates under aggressive environments. The uncoated substrates exhibited corrosion rates ranging from 24.378 to 58.125 mm year^{-1}, depending on the corrosive medium. After the application of the silicone oil coating, the corrosion rate decreased to 11.621–26.125 mm year^{-1}, corresponding to an improvement of approximately 50–55%. This reduction indicates that the silicone oil layer provides partial protection by forming a hydrophobic barrier that reduces direct contact between the metallic surface and the electrolyte. The incorporation of reduced graphene oxide (rGO) and nanochitosan further enhanced the corrosion resistance of the coating. The optimum performance was obtained at 0.3 wt% rGO, where the corrosion rates decreased to 2.15 mm year^{-1} in 3.5 wt.% NaCl, 4.21 mm year^{-1} in seawater, and 11.478 mm year^{-1} in 3 wt.% H_2SO_4, corresponding to reductions of approximately 90% compared with the uncoated substrates. The variation in corrosion rate as a function of rGO concentration in different corrosive media is presented in Figure 9.

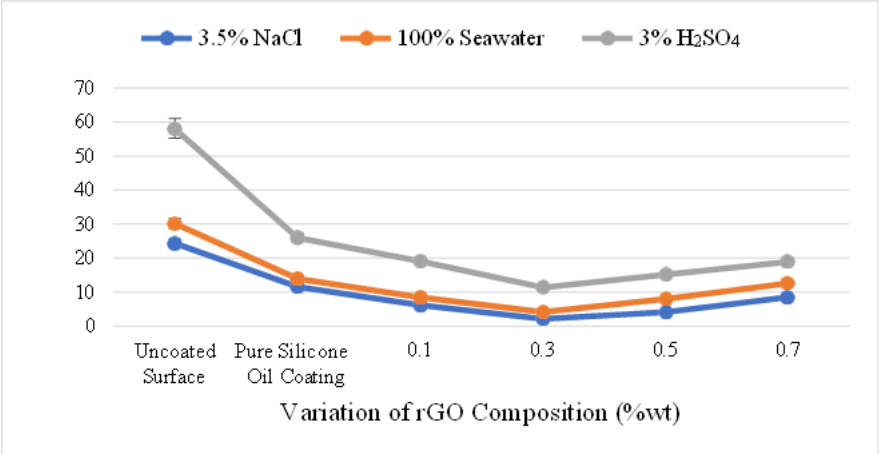

Figure 9. Effect of rGO concentration on the corrosion rate in different corrosive media: 3.5 wt.% NaCl, seawater, and 3 wt.% H_2SO_4.

As shown in Figure 9, the corrosion rate decreased progressively with increasing rGO concentration up to 0.3 wt%, followed by a gradual increase at higher concentrations. This trend is consistent with the tribological results and indicates that the optimum reinforcement content provides the most compact and homogeneous coating structure. The enhanced corrosion resistance is primarily attributed to the synergistic barrier effect of the silicone oil matrix, uniformly dispersed rGO nanosheets, and nanochitosan. Silicone oil acts as a hydrophobic matrix that reduces the penetration of the electrolyte into the coating. Meanwhile, the layered structure of rGO increases the diffusion path of aggressive species, including chloride ions, oxygen, moisture, and sulfate ions, thereby enhancing the barrier performance of the coating. Similar diffusion-barrier mechanisms have been widely reported for graphene-based protective coatings in corrosive environments [19]–[23], [49]. Nanochitosan further improves coating compactness and interfacial adhesion through its abundant hydroxyl (–OH) and amine ($–NH_2$) functional groups. The improved coating integrity minimizes coating defects and limits the transport of corrosive species toward the metallic substrate. Previous studies have similarly demonstrated that chitosan-based coatings enhance corrosion resistance by improving coating stability and forming compact protective films on metallic surfaces [30]–[33], [50].

However, increasing the rGO concentration beyond the optimum level (0.5–0.7 wt%) resulted in a gradual

increase in corrosion rate. This deterioration is attributed to the agglomeration of rGO nanosheets, which reduces coating homogeneity and introduces localized defects that facilitate electrolyte penetration. The effect becomes more pronounced in acidic environments, where the higher proton concentration accelerates corrosion processes. Similar observations have been reported for rGO/polymer nanocomposite coatings, where excessive rGO loading decreases corrosion resistance because of nanosheet agglomeration and coating discontinuity [24], [36]. Overall, the superior corrosion resistance achieved at 0.3 wt% rGO is attributed to the formation of a compact hybrid coating with homogeneous nanosheet dispersion, improved interfacial adhesion, and enhanced barrier properties. These characteristics effectively restrict the penetration of corrosive species and provide long-term protection for metallic substrates under different corrosive environments.

The corrosion performance discussed in this study is primarily based on corrosion rate measurements, which demonstrate the protective capability of the developed coating under different corrosive environments. Nevertheless, a more comprehensive electrochemical evaluation involving potentiodynamic polarization analysis, including corrosion potential (Ecorr) and corrosion current density (Icorr), together with electrochemical impedance spectroscopy (EIS), would provide deeper insight into the corrosion inhibition mechanism, charge-transfer behaviour, and coating/electrolyte interfacial characteristics [51], [52]. These complementary electrochemical analyses are recommended for future investigations to further validate the corrosion protection mechanism of the developed multifunctional coating system.

4. Conclusion

This study demonstrated that incorporating reduced graphene oxide (rGO) and nanochitosan into a silicone oil matrix effectively improved the tribological and corrosion performance of aluminium and copper substrates. The optimum formulation containing 0.3 wt% rGO reduced surface roughness, coefficient of friction, wear rate, and corrosion rate by approximately 40, 90, 86, and 90%, respectively, relative to the uncoated substrates. XRD analysis confirmed the characteristic structural features of rGO, nanochitosan, and the PDMS matrix, while the reduced apparent crystallite size and increased microstrain of the rGO phase indicated structural modification following incorporation into the matrix. The scientific contribution of this study is the demonstration of a structure–performance relationship in the rGO/nanochitosan-reinforced silicone oil system, showing that an optimum reinforcement concentration is critical for achieving balanced tribological and corrosion resistance. The 0.3 wt% rGO formulation therefore shows practical potential as a multifunctional surface treatment for metallic components operating under coupled mechanical and corrosive conditions, particularly in engineering and marine applications. Future studies should address long-term durability, coating adhesion strength, and advanced electrochemical characterization, particularly potentiodynamic polarization (Ecorr and Icorr) and electrochemical impedance spectroscopy (EIS), to further validate the protection mechanism and service stability of the developed system.

Acknowledgments

The authors gratefully acknowledge the financial support provided by the Think Efficiency Competition Program in Tribology Innovation, organized by Energy Academy Indonesia (ECADIN) under the Shell Indonesia Program. The authors also express their appreciation for the valuable support and contributions that enabled the completion of this research.

References

[1] K. Holmberg and A. Erdemir, "Influence of tribology on global energy consumption, costs and emissions," *Friction*, vol. 5, no. 3, pp. 263–284, 2017.

[2] K. Holmberg and A. Erdemir, "The impact of tribology on energy use and CO2 emission globally and in combustion engine and electric cars," *Tribology International*, vol. 135, pp. 389–396, 2019.

[3] H. Wang, X. Chen, C. Kang, Y. Tang, J. Sun, Z. Wang, et al., "Janus PVDF-modified melamine sponge composite for high-efficiency solar seawater desalination," *ACS Applied Polymer Materials*, vol. 7, no. 10, pp. 6427–6438, 2025.

[4] Z. Pan, C. Cai, and R. Liu, "Synthesis of a multifunctional silicone oil exhibiting high-temperature resistance and its application in high-temperature resistant lubricating oil," *Silicon*, vol. 17, no. 11, pp. 2559–2572, 2025.

[5] T. Aziz, H. Fan, F. U. Khan, M. Haroon, and L. Cheng, "Modified silicone oil types, mechanical properties and applications," *Polymer Bulletin*, vol. 76, no. 4, pp. 2129–2145, 2019.

[6] X. Luan, E. Zhang, Y. Chen, R. Ma, K. Gong, W. Li, and X. Wang, "Chemically modified silicone oil with enhanced tribological and anti-foaming properties," *Lubricants*, vol. 10, no. 12, p. 364, 2022.

[7] M. Venczel, G. Bognár, and Á. Veress, "Temperature-dependent viscosity model for silicone oil and

its application in viscous dampers," *Processes*, vol. 9, no. 2, p. 331, 2021.
[8] Z. Wang, G. Zhao, K. Gong, S. Liu, S. Bai, X. Wang, and Z. Xu, "Effect of different silicone oils on the tribological and rheological properties of nano-silica-based grease at high temperatures," *Industrial Lubrication and Tribology*, vol. 78, no. 5, pp. 844-854, 2026.
[9] T. Wang, J. Yang, S. Chen, Y. Sun, X. Jia, and H. Song, "Long-term stable superlubricity coatings enabled by the interaction between the polydimethylsiloxane brush and silicone oil," *ACS Applied Materials & Interfaces*, vol. 16, no. 8, pp. 11134-11144, 2024.
[10] A. Rosenkranz, Y. Liu, L. Yang, and L. Chen, "2D nano-materials beyond graphene: From synthesis to tribological studies," *Applied Nanoscience*, vol. 10, no. 9, pp. 3353–3388, 2020.
[11] G. Zhao, X. Li, M. Huang, Z. Zhen, Y. Zhong, Q. Chen, et al., "The physics and chemistry of graphene-on-surfaces," *Chemical Society Reviews*, vol. 46, no. 15, pp. 4417–4449, 2017.
[12] P. Raturi, "Graphene-Based Nanocomposites and Their Applications," in *Advances in Emerging Materials in Electronics, Energy, and Biotechnology: Fabrication, Characterization, and Applications*, S. Seo, S. Gupta, S. Kumar, and C. S. Pathak, Eds. Boca Raton, FL, USA: CRC Press, 2026, pp. 378–404. [Online]. Available: https://doi.org/10.1201/9781003581550.
[13] B. Jin, G. Chen, Y. He, C. Zhang, and J. Luo, "Lubrication properties of graphene under harsh working conditions," *Materials Today Advances*, vol. 18, p. 100369, 2023.
[14] S. Chen, B. Shen, Y. Chen, and F. Sun, "Synergistic friction-reducing and anti-wear behaviors of graphene with micro- and nano-crystalline diamond films," *Diamond and Related Materials*, vol. 73, pp. 25–32, 2017.
[15] X. Ye, X. Liu, Z. Yang, Z. Wang, H. Wang, J. Wang, and S. Yang, "Tribological properties of fluorinated graphene reinforced polyimide composite coatings under different lubricated conditions," *Composites Part A: Applied Science and Manufacturing*, vol. 81, pp. 282-288, 2016.
[16] D. Berman, S. A. Deshmukh, S. K. R. S. Sankaranarayanan, A. Erdemir, and A. V. Sumant, "Macroscale superlubricity enabled by graphene nanoscroll formation," *Science*, vol. 348, no. 6239, pp. 1118–1122, 2015.
[17] J. Sun and S. Du, "Application of graphene derivatives and their nanocomposites in tribology and lubrication: A review," *RSC Advances*, vol. 9, no. 69, pp. 40642–40661, 2019.
[18] M. Sarno, D. Scarpa, A. Senatore, and W. A. A. Mustafa, "rGO/GO nanosheets in tribology: From the state of the art to the future prospective," *Lubricants*, vol. 8, no. 3, p. 31, 2020.
[19] A. Sharma, and S. Sharma, "Graphene-based polymer coatings for preventing marine corrosion: A review," *Journal of Coatings Technology and Research*, vol. 20, no. 2, pp. 413-432, 2023.
[20] L. M. Muresan, "Nanocomposite coatings for anti-corrosion properties of metallic substrates," *Materials*, vol. 16, no. 14, p. 5092, 2023.
[21] M. S. Selim, S. A. El-Safty, M. A. Abbas, and M. A. Shenashen, "Facile design of graphene oxide-ZnO nanorod-based ternary nanocomposite as a superhydrophobic and corrosion-barrier coating," *Colloids and Surfaces A: Physicochemical and Engineering Aspects*, vol. 611, p. 125793, 2021.
[22] T. Liu, W. Lyu, Z. Li, S. Wang, X. Wang, J. Jiang, and X. Jiang, "Recent progress on corrosion mechanisms of graphene-reinforced metal matrix composites," *Nanotechnology Reviews*, vol. 12, no. 1, p. 20220566, 2023.
[23] H. Assad, I. A. Lone, A. Sihmar, A. Kumar, and A. Kumar, "An overview of contemporary developments and the application of graphene-based materials in anticorrosive coatings," *Environmental Science and Pollution Research*, vol. 32, no. 28, pp. 16958–16977, 2025.
[24] A. Zeinedini and M. M. Shokrieh, "Agglomeration phenomenon in graphene/polymer nanocomposites: Reasons, roles, and remedies," *Applied Physics Reviews*, vol. 11, p. 041301, 2024.
[25] M. A. Rahman, S. M. Hasnain, R. Zairov, and R. Kumar, "Recent advances in nanocomposites and nano-adsorbents for heavy metal and dye removal from water," *Cleaner Water*, vol. 5, p. 100215, 2026.
[26] M. Sharma, P. Kumar, and J. Singh, "Eco-friendly nanofillers as additives," in *Handbook of Nanofillers*, Singapore: Springer Nature Singapore, 2025, pp. 1709–1728.
[27] Y. D. Yolanda, F. Zahra, M. Nurhayati, and F. Khoerunnisa, "Synthesis and characterization of chitosan nanoparticles by ionic gelation method," in *Engineering Physics International Conference 2021 (EPIC 2021)*, vol. 2580, no. 1, p. 050017, AIP Publishing LLC, May 2023.
[28] L. Yang, X. Zhao, J. Zhang, S. Ma, L. Jiang, Q. Wei, M. Cai, and F. Zhou, "Synthesis of charged chitosan nanoparticles as functional biolubricant," *Colloids and Surfaces B: Biointerfaces*, vol. 206, p. 111973, 2021.
[29] A. H. Abdel-Salam and A. Morsy, "Development of cellulose acetate/nano chitosan-silver

nanoparticle mixed matrix membranes with enhanced water treatment and fouling resistance," *Polymer Engineering & Science*, vol. 66, no. 5, pp. 3665-3678, 2026.

[30] S. Shankar, S. Joshi, and R. K. Srivastava, "A review on heavy metal biosorption utilizing modified chitosan," *Environmental Monitoring and Assessment*, vol. 195, no. 11, p. 1350, 2023.

[31] O. A. A. Ali, M. E. Owda, M. M. Elsawy, and H. A. El-Wahab, "Utilization of ecofriendly organic nanomaterial based on prepared chitosan nanoparticles with outstanding corrosion resistance activity in primer coatings," *Pigment & Resin Technology*, vol. 55, no. 2, pp. 306-315, 2026.

[32] A. A. Aguilar-Ruiz, R. G. Sánchez-Duarte, V. M. Orozco-Carmona, G. E. Devora-Isiordia, Y. Villegas-Peralta, and J. Álvarez-Sánchez, J. "Chitosan and its derivatives as a barrier anti-corrosive coating of 304 stainless steel against corrosion in 3.5% sodium chloride solution," *Coatings*, vol. 14, no. 10, p. 1244, 2024.

[33] C. Verma, M. A. Quraishi, A. Alfantazi, and K. Y. Rhee, "Corrosion inhibition potential of chitosan based Schiff bases: Design, performance and applications," *International Journal of Biological Macromolecules*, vol. 184, pp. 135–143, 2021.

[34] M. Hamid, I. Dayana, D. Sholeha, M. F. Siregar, I. Roza, M. Rianna, and H. Wijoyo, "Eco-friendly utilization of chitosan from shrimp shells for used lubricating oil cleaning," *Results in Surfaces and Interfaces*, vol. 18, p. 100368, 2025.

[35] E. Akdaşçi, H. Duman, F. Eker, M. Bechelany, and S. Karav, "Chitosan and its nanoparticles: A multifaceted approach to antibacterial applications," *Nanomaterials*, vol. 15, no. 2, p. 126, 2025.

[36] H. P. Zhang, B. Yang, Z. M. Wang, C. Xie, P. Tang, L. Bian, F. Dong, and Y. Tang, "Porous graphene oxide/chitosan nanocomposites based on interfacial chemical interactions," *European Polymer Journal*, vol. 119, pp. 114-119, 2019.

[37] R. K. Mishra, S. Goel, and A. Sharma, "Multifunctional chitin, chitosan, and nano-chitosan composites for water purification, eco-friendly packaging, flexible electronics, clean energy, and biomedical solutions: A comprehensive review," *Polymer Bulletin*, vol. 83, no. 5, p. 269, 2026.

[38] S. Girish and P. Tambe, "Surfactant assisted exfoliation of high purity graphene in aqueous solution as a nanofluid using kitchen blender: Influence on dispersion, thermal conductivity and rheological properties," *Advanced Powder Technology*, vol. 33, no. 10, p. 103767, 2022.

[39] S. Hamze, D. Cabaleiro, and P. Estellé, "Graphene-based nanofluids: A comprehensive review about rheological behavior and dynamic viscosity," *Journal of Molecular Liquids*, vol. 325, p. 115207, 2021.

[40] B. Luo, X. Wang, H. Sun, and L. Li, "Dielectric, ferroelectric, and thermodynamic properties of silicone oil modified PVDF films for energy storage application," *Applied Physics Letters*, vol. 108, no. 24, 2016.

[41] Y. Jiang, Z. Zhang, and Y. Qi, "The compatibility of three silicone oils with polydimethylsiloxane and the microstructure and properties of their composite coatings," *Polymers*, vol. 13, no. 14, p. 2355, 2021.

[42] A. M. Kumar, M. A. Hussein, B. Suresh, S. Ramakrishna, S. Saravanan, and M. Javid, "Multifunctional poly (lactic acid)/vanillin coatings on drug loaded titanium nanotube arrays for improved biocompatibility, corrosion resistance, and antibacterial characteristics," *Scientific Reports*, vol. 15, no. 1, p. 32844, 2025.

[43] N. J. Tamanna, M. S. Hossain, N. M. Bahadur, and S. Ahmed, "Green synthesis and characterization of silver (Ag) nanoparticles: Crystallographic analysis from X-ray diffraction," *Chemistry of Inorganic Materials*, vol. 8, p. 100144, 2026.

[44] K. M. Kumar, P. V. Shanmuganathan, and A. Sethuramiah, "Tribology of silicon surfaces: A review," *Materials Today: Proceedings*, vol. 5, no. 11, pp. 24809–24819, 2018.

[45] R. Leach, H. Haitjema, R. Su, and A. Thompson, "Metrological characteristics for the calibration of surface topography measuring instruments: A review," *Measurement Science and Technology*, vol. 32, no. 3, p. 032001, 2021.

[46] J. Guegan, M. Southby, and H. Spikes, "Friction modifier additives, synergies and antagonisms," *Tribology Letters*, vol. 67, no. 3, p. 83, 2019.

[47] L. H. Prado *et al.*, "Silicone-based lubricant-infused slippery coating covalently bound to aluminum substrates for underwater applications," *ACS Applied Materials & Interfaces*, vol. 15, no. 26, pp. 31776–31786, 2023.

[48] Z. Yu, A. T. Lim, S. L. Kollasch, H. D. Jang, and J. Huang, "Oil-based self-healing barrier coatings: To flow and not to flow," *Advanced Functional Materials*, vol. 30, no. 2, p. 1906273, 2020.

[49] N. Anis, C. Lai, and B. Ong, "A review of graphene oxide crosslinking as enhanced corrosion shield

application," *Journal of Renewable Materials*, vol. 11, no. 6, p. 2745, 2023.
[50] A. Murari, A. Arathi, U. Sirimahachai, S. Rao, and G. Hegde, "Corrosion inhibition of mild steel using eco-friendly porous nanocarbon derived from waste mango kernels: A step towards sustainability," *RSC Advances*, vol. 16, no. 8, pp. 6915–6930, 2026.
[51] N. Li, H. Wang, Q. Liu, Z. Hao, D. Xu, X. Chen, et al., "Review of preparation and key functional properties of micro-arc oxidation coatings on various metal substrates," *Coatings*, vol. 15, no. 10, p. 1201, 2025.
[52] F. M. Li, L. Huang, S. Zaman, W. Guo, H. Liu, X. Guo, and B. Y. Xia, "Corrosion chemistry of electrocatalysts," *Advanced Materials*, vol. 34, no. 52, p. 2200840, 2022.